Sensors & Diagnostics

PAPER

View Article Online
View Journal | View Issue

Cite this: *Sens. Diagn.*, 2024, **3**, 1522

Highly efficient WS_2 QD-based non-enzymatic fluorescent biosensor for ofloxacin and ciprofloxacin monitoring in aquatic media†

Sunayana Bora * and Chandan Upadhyay

Quantum dot-based biosensors have gained prominence in recent times for the detection of biological and chemical hazards present in aquatic media which essentially contribute to the degradation of the environment and human health. Within this work, we demonstrate a WS_2 QD-induced turn-on fluorescent probe for specific monitoring of ofloxacin (OFL) and ciprofloxacin (CIP) residues in water. An efficient one-pot hydrothermal approach is applied for fluorescent water-soluble WS_2 QD preparation. The WS_2 QDs possess excellent photostability and monodispersity along with a superior shelf life. The WS_2 QDs interacting with FQns (OFL and CIP) showed a systematically enhanced fluorescence in varying FQn concentrations from 0 μM to 3 μM. Also, all the measurements showed excellent results for sensitivity along with superior specificity as well as anti-interference ability over other interfering substances like various metal ions and antibiotic derivatives. The proposed sensor allows the quantification of FQns in the range of 0–3 μM with the lowest detectable amount (LOD) of 0.08 μM and 0.06 μM and the minimal limit of quantification (LOQ) of 0.26 μM and 0.21 μM for both OFL and CIP, respectively, at natural pH. It achieved higher sensitivity than many established techniques and materials making up the gap of other existing systems in this range. We observed excellent results for the rapid *in situ* detection of FQns by implementing WS_2 QDs. The findings show potential for future use in real-time applications for FQns.

Received 10th May 2024,
Accepted 20th July 2024

DOI: 10.1039/d4sd00148f

rsc.li/sensors

Introduction

While groundwater supplies approximately half of the world's residential water requirements, surface water serves as the habitat and sustenance of amphibians and aquatic species.[1] Evolving consumption patterns, especially in diet and socio-economic development, are driving the annual growth in the use of freshwater resources by just under 1%.[2] The rise in urban population, witnessing a 17% growth every decade, is predominantly accountable for the water pollution caused by industrial wastewater.[3] Due to the rise in demand for water, it is very important to monitor the quality of water for use. One of the major sources of water pollution is pharmaceutical waste. Pharmaceutical active compounds (PACs) are frequently used to treat and avoid several infections affecting humans and other animals. Residues of these PACs are recognized as emerging micropollutants that enter aquatic ecosystems, causing risks of harmful ecotoxicity.[4,5] One of the major contaminants of water is antibiotics.[6] Numerous antibiotic substances, including macrolides, quinolones, sulfonamides, and tetracyclines, are widely utilized for treating infections in livestock farming and human health.[6,7] Exposure to these substances may lead to either acute or prolonged detrimental outcomes, creating potential hazards to consumers' health, including some adverse effects like harm to the kidneys, carcinogenicity, aberration in reproductive function, allergy, and immunopathogenic response.[6,8] Furthermore, the utilization of antibiotics has increased the frequency of resistance genes, which has posed a global threat to public health.[9] Yet, the excessive usage of antibiotics leads to some adverse consequences for both the ecosystem and human health through manure and other discharges.[10–12]

Fluoroquinolones (FQns, Fig. 1) that come from quinolone derivatives predominantly pollute the water due to their

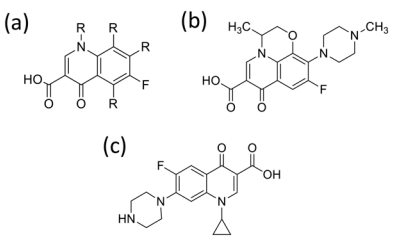

Fig. 1 Chemical structures of (a) fluoroquinolones (FQns), (b) ofloxacin (OFL), and (c) ciprofloxacin (CIP).

School of Materials Science and Technology, Indian Institute of Technology (Banaras Hindu University), Varanasi – 221005, Uttar Pradesh, India.
E-mail: sunayanabora.rs.mst21@iitbhu.ac.in, Sunayanabora01@gmail.com

† Electronic supplementary information (ESI) available. See DOI: https://doi.org/10.1039/d4sd00148f

extensive use in human medicines along with animal husbandry, aquaculture, and various farming industries.[13,14] Ciprofloxacin and ofloxacin (Fig. 1) are second-generation fluoroquinolone antibiotics that belong to the broad-spectrum category and are known for their effectiveness and resistance, and both are extensively used in treating bacterial pathogen-related diseases in humans and animals due to their extensive antibacterial activity spectrum and effortless oral intake.[13–17] The extensive use of ciprofloxacin and ofloxacin in humans and veterinary medicine can generate unavoidable adverse effects on the natural surroundings and health of individuals. Also due to poor biodegradation properties, they remain unmetabolized, and are discharged routinely into the environment, soil and water bodies such as ground and surface water in the form of urine, sewage, pharmaceutical wastewater, and various other domains, inducing potential impacts on human health and ecosystems due to environmental and water pollution.[18–22] Even at extremely low concentrations, these substances can cause prolonged absorption, thus resulting in the appearance of their residues in human entities through the food web causing a potential public health risk like liver damage and central nervous system injury.[18,19,21,23] As a result, the presence of FQn (OFL and CIP) residues leads to serious concerns about the environmental and human well-being worldwide.[24] Consequently, it is essential to establish a prompt, sensitive, and reliable approach for detecting FQns like ofloxacin and ciprofloxacin antibiotics.[25–27]

Several materials, like metal–organic frameworks (MOFs), carbon-based materials, metallic nanoparticles, transition metal dichalcogenides (TMDs), quantum dots (QDs), *etc.*, have been already developed for antibiotic detection in water but still, their real-time application in the field is a challenging task. So, the development of effective materials for this purpose is highly in demand. Among all these materials, TMD quantum dots (TMD QDs) show very satisfactory results towards antibiotic detection due to their excellent properties. Transition metal dichalcogenides (TMDs) represent a category of semiconductive substances resembling the structure of graphene. Resulting from the quantum confinement and the edge effect, TMDs show exceptional photoluminescence properties. These materials find widespread applications in bioimaging, sensors, catalysis, and electronic and optical devices. Bulk TMDs exhibit a layered structure of hexagonal geometry, with the layer consisting of an S–M–S sandwich-like structure covalently bonded by chalcogen atoms and metal atoms strongly.[28] Furthermore, these layers are held together by a weak intermolecular force of attraction identified as the van der Waals force. In comparison to graphene's zero-band gap characteristics, the switching from an indirect band gap to a direct energy barrier induced by the TMD exfoliation and transformation from bulk to a layered arrangement enhances their suitability for diverse applications involving semiconductor-driven electronic and optical equipment, sensors, catalysis, and bioimaging. When the dimensions of TMDs are reduced to below 10 nm (<10 nm), the creation of TMD quantum dots (TMD QDs) is achieved. The photoluminescence achievement of TMD QDs experiences a significant enhancement considering the quantum confinement and edge effect.[29,30] Among TMDs, molybdenum disulfide (MoS_2) as an extensively researched material has achieved considerable progress, whereas some alternative TMD QDs including molybdenum diselenide ($MoSe_2$), tungsten disulfide (WS_2), as well as tungsten diselenide (WSe_2) QDs have yet to be explored and the exploration remains a challenging task. WS_2 QDs, like MoS_2 QDs, have outstanding photoluminescence properties, are easy to prepare, and exhibit fine water solubility and also a biocompatible nature, along with minimal toxicity, and thus all these features make them appealing substances for applications as biosensors.[10,31,32]

In the course of this study, we successfully synthesized WS_2 QDs by employing a straightforward single-step hydrothermal approach utilizing $Na_2WO_4{\cdot}2H_2O$ and L-Cysteine (L-Cys) as starting materials. Furthermore, the WS_2 QDs were observed to possess a crystalline nature with a very small size of approximately ~2.5 nm. Also, these synthesized WS_2 QDs are monodispersed and soluble in water. The FL probe confirmed that WS_2 QDs can serve as an extremely sensitive, selective, and viable fluorescent sensor to identify 2nd generation FQns that are OFL and CIP, with LODs as low as 0.08 μM and 0.26 μM, respectively. Also, their LOQs were observed to be 0.06 μM and 0.21 μM for OFL and CIP, respectively.

Experimental section

Chemicals and materials

Sodium tungstate ($Na_2WO_4{\cdot}2H_2O$), L-Cysteine (L-Cys), and $FeCl_2$ were purchased from Sisco Research Laboratories Pvt. Ltd. (SRL)-India. KCl, NaCl, and $CaCl_2$ were purchased from Loba Chemie Pvt. Ltd., Mumbai, India. All the antibiotics used in this work were purchased from local medical stores in Varanasi, India. Dialysis membranes (av. flat width – 28.46, av. diameter – 17.5 mm) were acquired from Himedia Laboratories Pvt. Ltd. All the reagents utilized in the experiment met the analytical grade standard; also, we applied double distilled water throughout the entire reaction process.

Apparatus

The fluorescence spectra were collected on a Hitachi F-4600 fluorescence spectrophotometer. X-ray diffraction measurement was performed on a Rigaku Miniflex 600 desktop X-ray diffraction system. The transmission electron microscopy (TEM) pictures were obtained with a Tecnai G2 20 TWIN (EDAX Inc.). UV-vis spectra were obtained on an EPOCH 2, USA, Biotek spectrophotometer. The FTIR spectra were captured on a ThermoScientific Nicolet Summit FTIR spectrometer.

Preparation of WS_2QDs

WS_2 QDs were prepared under straightforward single-step hydrothermal conditions by modifying the reported method.[33] Here, we used a W-to-S molar ratio of 1 : 6. Sodium tungstate ($Na_2WO_4{\cdot}2H_2O$) (0.45 g) was finely solubilized in 45 mL water to make a clear solution and L-Cys (0.65 g) was solubilized in 30 mL of water to prepare a separate solution. Subsequently, both of these solutions were properly intermixed and the resulting reaction solution was placed into a 100 mL Teflon-lined stainless-steel autoclave and kept heating at ~200 °C for 8 h using a hot air oven followed by cooling the reaction mixture at ambient temperature. Subsequently, this cooled reaction mixture was centrifuged at 8000 rpm for about 20 minutes. The pale-yellow supernatant liquid was collected. Some of this liquid was dialyzed to remove any kind of impurities and stored for future use. The rest of the product was dried at 60 °C, and pale-yellow powder of WS_2 QDs was collected and stored at 4 °C. A schematic representation of the synthesis method for WS_2 QDs is shown in Fig. S1.†

Preparation of ofloxacin and ciprofloxacin antibiotic solution

Ofloxacin and ciprofloxacin antibiotics were procured from local medical stores in Varanasi, India, and they were ground well to make fine powder and stored in a refrigerator for further use. 10 mL of 0.001 M stock solutions of both OFL and CIP were prepared and from these solutions, several concentrations ranging from 0 μM to 3 μM for both the OFL and CIP solutions were prepared and used for detection in water.

Fluorescence assessment

The method for applying WS_2 QDs as a fluorescent sensor for the detection of FQns (OFL and CIP) in water is given as follows. A fixed amount of WS_2 QDs (50 μL) mixed with various concentrations (0 μM to 3 μM) of OFL was added in 2.5 ml of water at room temperature, and the fluorescence spectra were measured. Similarly, a particular concentration range from 250 nM to 3 μM of CIP and 50 μL of WS_2 QDs were added in 2.5 mL of DI water for monitoring the fluorescence spectra. The FL spectra for both of the antibiotics were acquired on a Hitachi F-4600 fluorescence spectrophotometer at an excitation wavelength of 310 nm. The excitation and emission slits were positioned at 1 nm and 5 nm, respectively.

Characterization of WS_2 QDs

The acquired WS_2 QDs were characterized by employing XRD, TEM, FT-IR, UV-vis, and fluorescence techniques. From the X-ray diffraction (XRD) pattern of WS_2 QDs (Fig. 2(a)), we observed XRD peaks at 2θ = 15.08°, 30.72°, and 46.98° corresponding to the diffraction peaks of the (002), (100), and (105) lattice planes of WS_2 QDs as per the reported work.[27,34] The synthesized WS_2 QDs were further

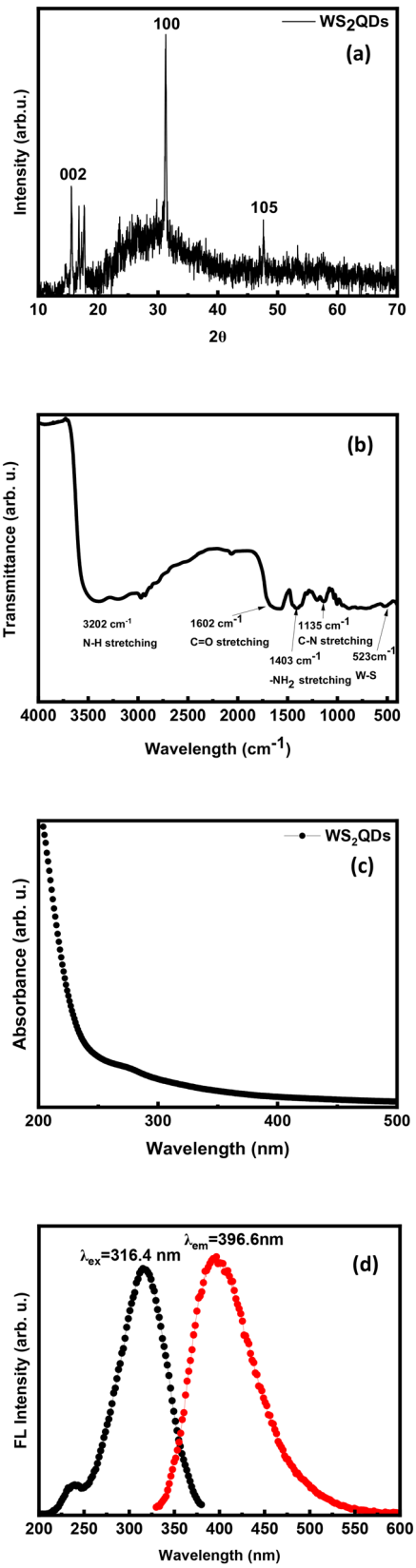

Fig. 2 (a) The XRD pattern of WS_2 QDs, (b) FTIR spectrum of WS_2 QDs, (c) UV-visible absorption spectrum of WS_2 QDs, and (d) fluorescence excitation and emission spectra of WS_2 QDs.

verified by FTIR to determine the functional moieties existing on the surface. As shown in Fig. 2(b), the peak around 3202 cm^{-1} is correlated to the stretching of the O–H group, the peak at 1602 cm^{-1} is linked to C═O stretching, the peak at 1403 cm^{-1} denotes $–NH_2$ stretching and the peak at 1135 cm^{-1} denotes C–N stretching. As WS_2 contains $–NH_2$ and –COOH groups, it had outstanding solubility in water. Furthermore, the weak peak that appeared around 523 cm^{-1} refers to the distinctive peak of W–S, and the specific peak for the S–H stretching band at 2583 cm^{-1} dissipated; the complete set of observed data indicates that the WS_2 QDs have been prepared successfully. Fig. 2(c) displays the UV-vis absorption spectrum of WS_2 QDs, which shows peaks in the UV region in correspondence with the excitonic feature. The bandgap of WS_2 QDs is larger (3.86 eV) in comparison to that of the WS_2 monolayer (1.98 eV).[30] The possible justification for this larger bandgap can be attributed to the greater quantum confinement effect resulting in the change in the dimension of the quantum dots formed, which is able to improve the spin-valley coupling.[29,30,35] The intense UV absorption of the WS_2 QDs indicates their potential for exhibiting FL emission. Fig. 2(d) shows the fluorescence excitation and emission spectra of WS_2 QDs, in which the maximum excitation and emission peaks were observed at 316.4 nm and 396.6 nm, respectively. So, a Stokes shift is observed here. The size distribution of WS_2 QDs was measured by the transmission electron microscopy (TEM) technique. It is observed from Fig. 3(a) that WS_2 QDs have good monodispersity and a relatively uniformly distributed particle size from 1.25 to 4.25 nm and the average particle size was ~2.5 nm. The prepared WS_2 QDs are mostly of spherical-like shape. The size distribution histograms were determined with 226 QDs by using ImageJ software, and are shown in Fig. 3(b). Fig. 3(c) displays the selected area electron diffraction (SAED) structure of WS_2 QDs. The SAED pattern having an aureole reveals that the as-synthesized WS_2 QDs exhibit a polycrystalline nature.[36]

The FL spectra of WS_2 QDs were obtained with an excitation wavelength from 280 to 340 nm (Fig. 4(a)). It is observed from the FL spectra (Fig. 4(a)) that the peak intensity is increasing gradually and then starts to decrease gradually after reaching the maximum value of the emission peak at a wavelength of 396 nm at an excitation wavelength of 310 nm. Additionally, the shifting of the peak is also observed at the maximum emission peak position. By changing the excitation wavelength from 280 nm to 310 nm, the FL spectra of WS_2 QDs show an increase in FL intensity reaching a maximum value at 396 nm. By further raising the excitation wavelength from 310 nm to 340 nm, the FL emission peaks of WS_2 QDs started shifting gradually from 400 nm to 408 nm. This indicates that the obtained WS_2 QDs are dependent on the excitation wavelength and show size-dependent emission corresponding to different band gaps. Notably, the FL emission peak shows redshifts as the excitation wavelength increases. This phenomenon is attributed to the selective excitation of lower energy states like bound excitonic emissions.[37,38]

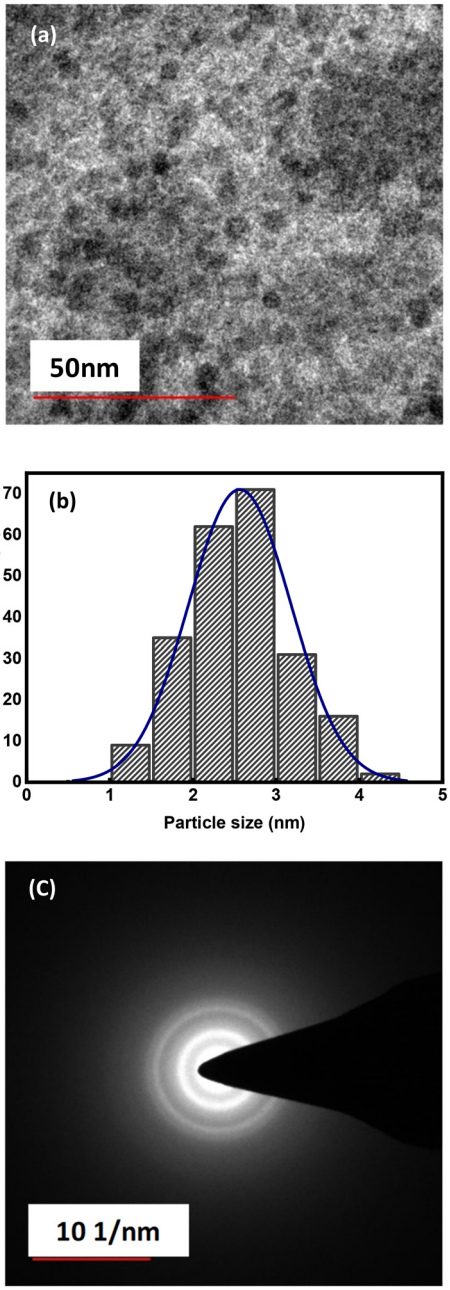

Fig. 3 (a) TEM image of WS_2 QDs, (b) size distribution histogram of WS_2 QDs, and (c) selected area electron diffraction (SAED) pattern of WS_2 QDs.

From Fig. 2(d), it is observed that the FL spectra of WS_2 QDs indicate excitation and emission peaks at maximum wavelengths of 316.4 nm and 396.6 nm, respectively, on account of the edge effect as well as the quantum confinement effect of 0-dimensional transition metal dichalcogenides (TMDs). The as-prepared WS_2 QDs showed good photoluminescence properties. During the experiment, WS_2 QDs were continuously irradiated at an excitation wavelength of 310 nm for 1 h, and we observed that the FL

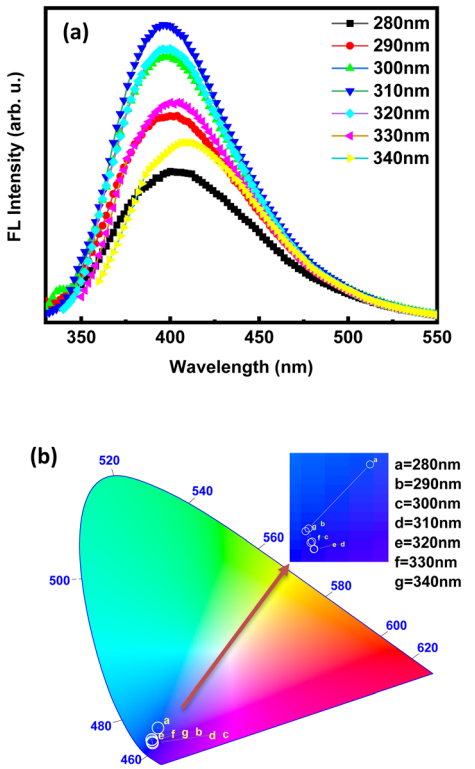

Fig. 4 (a) FL spectra of WS_2 QDs, (b) CIE chromaticity diagram of WS_2 QDs; excited at various wavelengths from 280 nm to 340 nm; inset: zoomed view of the CIE coordinates.

intensity of WS_2 QDs has good light stability as well as strong photobleaching resistance. Fig. 4(b) shows the CIE chromaticity coordinates of WS_2 QDs. WS_2 QDs displayed a range of emission wavelengths covering blue light. The standard CIE coordinates are (0.17, 0.11), (0.15, 0.08), (0.15, 0.07), (0.15, 0.67), (0.15, 0.06), (0.15, 0.07), and (0.15, 0.08) for 280 nm, 290 nm, 300 nm, 310 nm, 320 nm, 330 nm and 340 nm, respectively, aligned with the colour temperature from 1841 K to 8560 K.

Fluorescence detection of FQn antibiotics

Antibiotics play a crucial role in the environment and human well-being, so it is essential to determine whether WS_2 QDs can function in the form of fluorescent sensors for antibiotics. When doxycycline, amoxicillin, norfloxacin, ofloxacin, and ciprofloxacin were added to WS_2 QDs, only OFL, CIP, and NFX have been observed to have a substantial fluorescence enhancement effect on WS_2 QDs, indicating that WS_2 QDs could selectively detect FQns, namely OFL, CIP, and NFX. Fluorescence resonance energy transfer (FRET) may occur from WS_2 QDs to OFL, CIP, and NFX, resulting in FL enhancement of the WS_2 QDs. To investigate the performance of WS_2 QDs for detecting FQns (OFL, CIP, and NFX), FQns with different concentrations were added to the WS_2 QD solution. Although NFX shows comparatively less changes than the other two FQns (OFL and CIP), it can still be detected by using WS_2 QDs selectively. Here, we are giving an elaborate discussion only on OFL and CIP detection in water. The final concentration range of FQns was 0 μM to 3 μM. As shown in Fig. 5(a) and Fig. 6(a), the FL intensity of the WS_2 QDs showed a gradual enhancement with the gradual increase of OFL and CIP concentrations. To delve deeper into the correlation between the effect of enhancement and concentration of OFL and CIP, graphs of the FL emission peak position *versus* OFL and CIP concentration were obtained.

Fluorescence detection of ofloxacin by WS_2 QDs

Fig. 5(a) and (b) show the enhancement and shifting of the peak position of the FL emission spectra of WS_2 QDs on the addition of ofloxacin. The FL enhancement associated with the hydrogen bond interaction is accompanied by charge transfer between WS_2 QDs and ofloxacin by forming a charge transfer complex or a chelate complex.[25] This is due to the reason that ofloxacin can form metal complexes as it has the capacity to bind metal ions.[39,40] So here, ofloxacin may act as a ligand which can be either monodentate or bidentate and is capable of forming a coordination complex structure through dative bonds. When the concentration of ofloxacin increases from 0 to 3 μM gradually, the FL intensity of WS_2 QDs also increases along with shifting the emission peaks towards higher wavelengths upon excitation at a wavelength of 310 nm. Additionally, the interaction of OFL with the WS_2 QDs can alter the electronic structure and enhance the fluorescence. The specific mechanism of this interaction likely involves changes in charge transfer or surface chemistry. The antibiotic likely preferentially excites the lower energy states (bound excitons) due to specific interactions at the WS_2 QD surface. As a result, fluorescence emission from these selectively excited states contributes to the enhanced peak. The interaction between ofloxacin and WS_2 QDs involves charge transfer and changes in surface chemistry. These alterations affect the energy levels of the QD states, influencing the fluorescence behaviour. As the ofloxacin concentration rises, it interacts with the WS_2 QDs. The exact mechanism could involve charge transfer, surface passivation, or changes in energy levels. The shift toward higher wavelengths in the emission peaks is also noteworthy. When excited at 310 nm, the QDs emit light at longer wavelengths (lower energies). This redshift suggests that the QD energy levels are affected by the presence of OFL. The plot illustrating ofloxacin concentration *versus* FL emission intensity shows linearity in the concentration range from 0.0–3.0 μM (Fig. 5(c)). This satisfies the linear equation $y = mx + c$, *i.e.* $y = (21\,958.97) + (1521.77) \times x$; the intercept was 21 958.97 ± 40.54 and the slope value is 1521.77 ± 25.41. The detection limit was found to be 0.08 μM (=80 nM) and the minimum quantification limit (LOQ) was observed as 0.26 μM (=260 nM). In Fig. 5(c), the *y*-axis, denoting the FL intensity is plotted for better interpretation of data. Fig. 5(d) shows the contribution of both the charge transfer

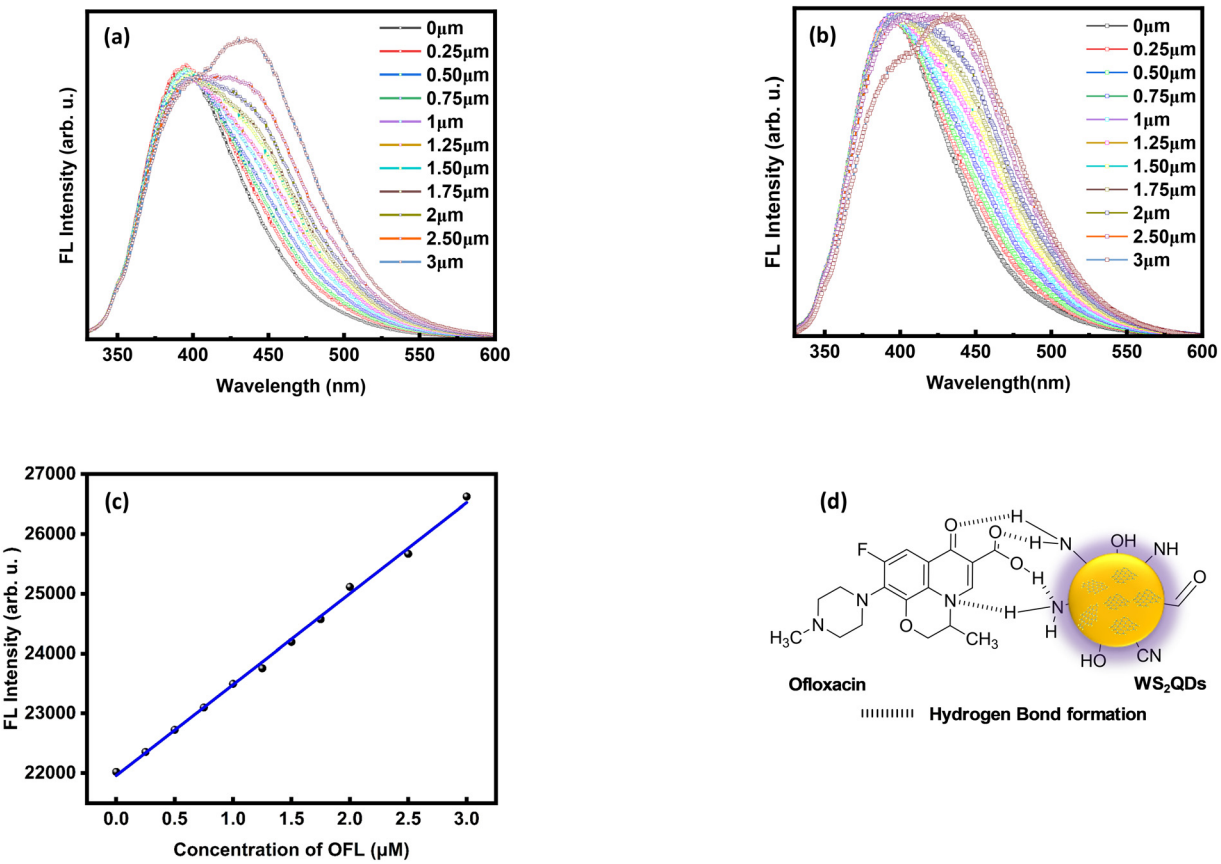

Fig. 5 (a) FL emission spectra of WS_2 QDs with the varying concentration range of OFL from 0 μm to 3 μM; (b) normalized FL emission of WS_2 QDs with the OFL concentration range from 0 μm to 3 μM; (c) OFL concentration *vs.* FL emission intensity of WS_2 QDs; (d) hydrogen bond formation between OFL and WS_2 QDs.

mechanism and hydrogen bonding formation ability. The standard CIE coordinates are (0.158, 0.065), (0.157, 0.071), (0.156, 0.074), (0.156, 0.079), (0.155, 0.083), (0.155, 0.086), (0.155, 0.088), (0.154, 0.09), (0.154, 0.092), (0.154, 0.095) and (0.153, 0.098) for 0 μM, 0.25 μM, 0.50 μM, 0.75 μM, 1.0 μM, 1.25 μM, 1.50 μM, 1.75 μM, 2.0 μM, 2.50 μM and 3.0 μM, respectively, corresponding to the colour temperature from 1801 K to 2777 K (Fig. 7(a)).

Fluorescence detection of ciprofloxacin by WS_2 QDs

Fig. 6(a) and (b) show the enhancement and peak shift of the FL emission spectra of WS_2 QDs following the insertion of ciprofloxacin. The FL enhancement associated with the hydrogen bond interaction is accompanied by charge transfer between WS_2 QDs and ciprofloxacin by forming a charge transfer complex.[25,39,40] Similar to ofloxacin, ciprofloxacin can also form a coordination complex with WS_2 QDs in an analogous manner. When the concentration of ciprofloxacin increases from 0 to 3 μM gradually, the FL intensity of WS_2 QDs also increases along with shifting the emission peaks towards higher wavelengths upon excitation at a wavelength of 310 nm. The observation revealed that the plot of CIP concentration *versus* FL emission intensity obeyed the behaviour of a linear relationship in the concentration range from 0.0–3.0 μM (Fig. 6(c)). The equation is $y = mx + c$ *i.e.* $y = (22\,278.10) + (4393.26) \times x$. The intercept was 22 278.11 ± 92.45 and the slope value is 4393.26 ± 55.25. The detection limit was determined to be 0.06 μM (=60 nM) and the minimum quantification limit (LOQ) was 0.21 μM (=210 nM) with a dynamic range of 0.0 μM to 3.0 μM. In Fig. 6(c), the graph is plotted to denote FL intensity values at the *Y*-axis for visual interpretation of data. Fig. 6(d) shows the contribution of both the charge transfer mechanism and hydrogen bonding formation ability. The standard CIE coordinates are (0.158, 0.068), (0.158, 0.066), (0.158, 0.064), (0.158, 0.063), (0.157, 0.062), (0.158, 0.06), (0.157, 0.06), (0.158, 0.058), (0.158, 0.058), (0.158, 0.056) and (0.158, 0.054) for 0 μM, 0.25 μM, 0.50 μM, 0.75 μM, 1.0 μM, 1.25 μM, 1.50 μM, 1.75 μM, 2.0 μM, 2.50 μM and 3.0 μM, respectively, corresponding to the colour temperature from 1829 K to 1733 K (Fig. 7(b)).

Selectivity/specificity and interference study of the WS_2 QD sensor

Because of the real sample composition's complexity, the presence of coexisting components might impact the

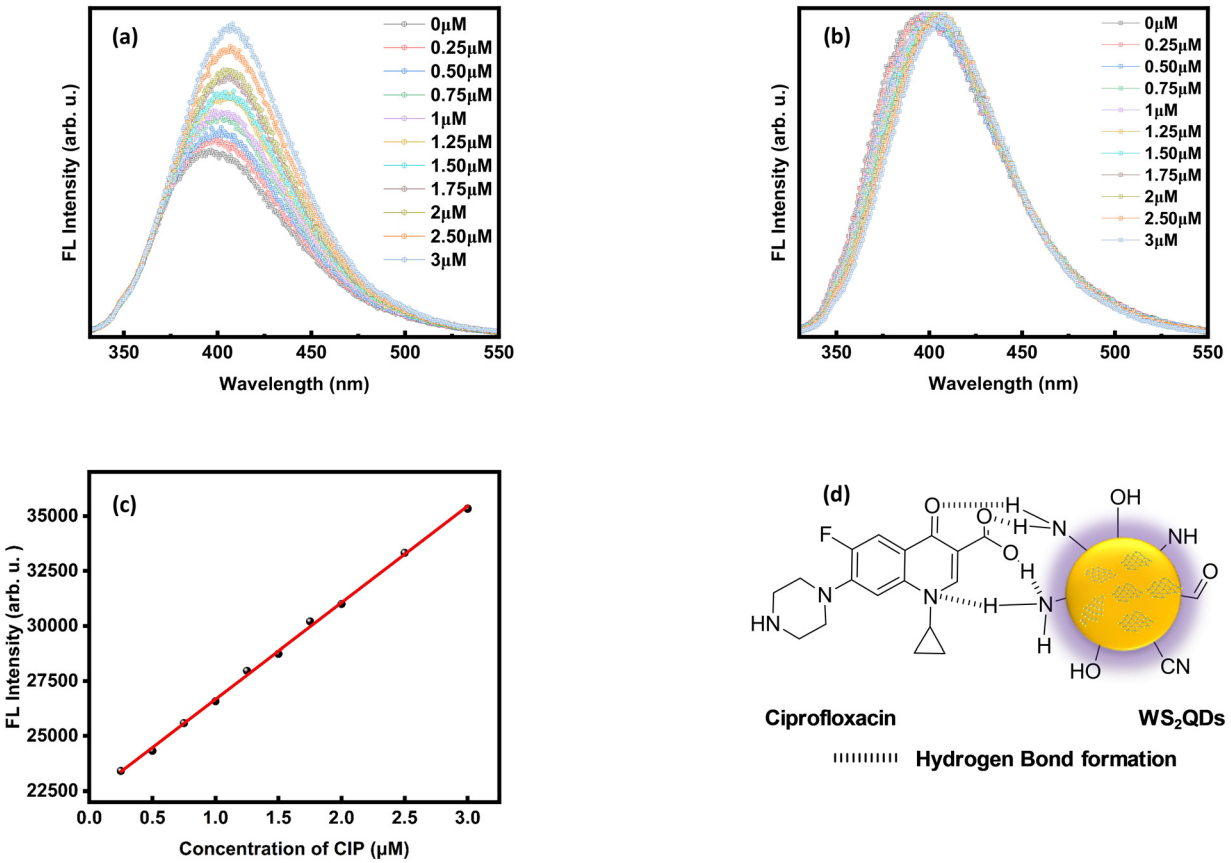

Fig. 6 (a) FL emission spectra of WS_2 QDs with the varying concentration range of CIP from 0 μm to 3 μM; (b) normalized FL emission of WS_2 QDs with the CIP concentration range from 0 μm to 3 μM; (c) CIP concentration *vs.* FL emission intensity of WS_2 QDs; (d) hydrogen bond formation between CIP and WS_2 QDs.

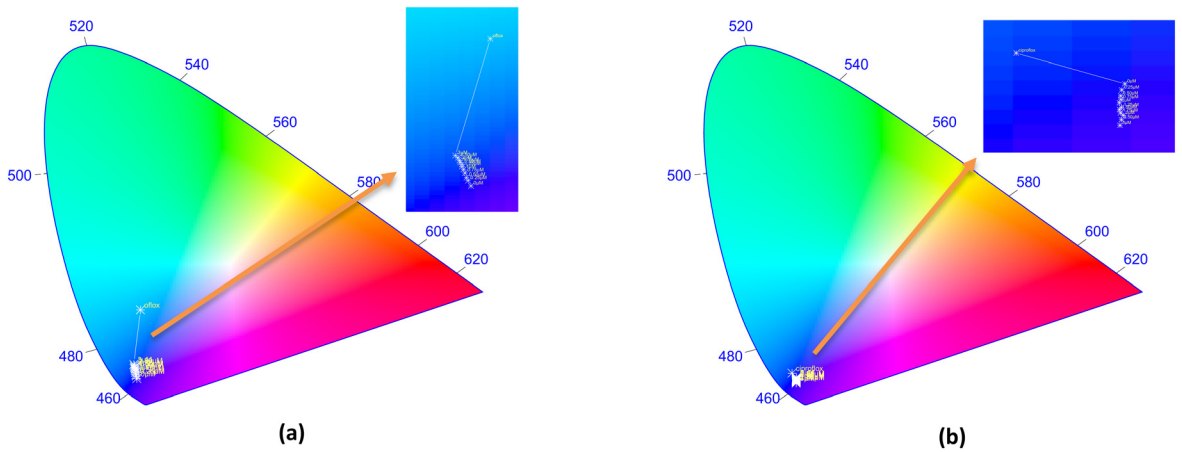

Fig. 7 (a) CIE chromaticity diagram of WS_2 QDs with OFL at different concentrations (0 μM to 3 μM); (b) CIE chromaticity diagram of WS_2 QDs with CIP at different concentrations (0 μM to 3 μM); with their respective color temperature.

determination of the fluoroquinolones (such as ofloxacin, ciprofloxacin, and norfloxacin) in water. For that reason, the selectivity and interference study of WS_2 QDs is important for evaluating the viability of this method. To investigate the selectivity for the detection of antibiotics including fluoroquinolone antibiotics namely ofloxacin, ciprofloxacin, and norfloxacin, as well as some other antibiotic derivatives such as amoxicillin, azithromycin, chloramphenicol, clarithromycin, doxycycline, and lincomycin, and some metal ions ($CaCl_2$, NaCl, KCl, $FeCl_2$) were used as substances. These substances were added to the WS_2 QD system at the same concentration (20 μM). Fig. 8(a) displayed that the

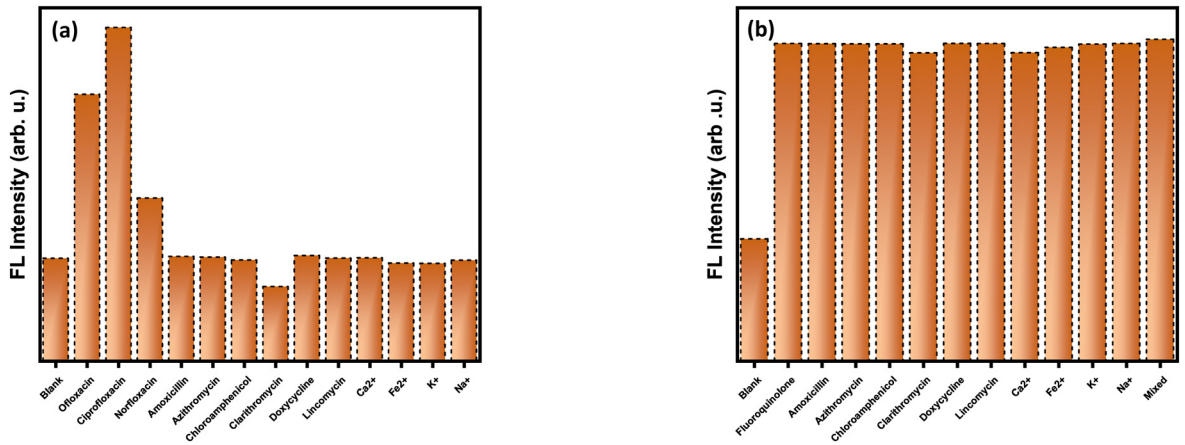

Fig. 8 (a) Effect of different antibiotics and other substances on specific detection of FQns by WS_2 QD assay; (b) interference study of FQn detection with WS_2 QDs in the presence of other interferent substances.

fluorescence intensity (and the peak position) of WS_2 QDs did not appear to change when other substances other than fluoroquinolone derivatives were present in the solution. As shown in Fig. 8(a), only FQns (OFL, CIP, and NFX) among all other antibiotics and other substances tested were able to show a significant change in the fluorescence spectra. A sample by mixing all the substances was also tested which shows a similar fluorescence change of pure fluoroquinolones.

Furthermore, we have investigated the influence of interferents on the WS_2 QD system with 20 μM of fluoroquinolone (OFL) antibiotics. Fig. 8(b) shows that these interference substances also had no evident interferences on fluoroquinolone (OFL) detection. When the fluoroquinolone concentration was 20 μM, the degree of FL enhancement of WS_2 QDs did not apparently change with the existence of other substances (amoxicillin, azithromycin, chloramphenicol, clarithromycin, doxycycline, and lincomycin; $CaCl_2$, NaCl, KCl, and $FeCl_2$) in the system. To test the anti-interference ability, a mixed interference system containing all of these substances was also arranged. As illustrated in the diagram (Fig. 8(b)), the fluorescence emission intensity increased dramatically and shifted in response to the same amount of FQns. That is, this developed sensor responded similarly in the mixed substance solution as it did in the pure FQn solution. This suggests that this method has superior specificity as well as anti-interference ability for second-generation FQn detection.

Other areas to use WS_2 QD-based sensors

WS_2 QD-based sensors exhibit unique properties that make them suitable for a variety of applications beyond antibiotic detection. Due to their unique fluorescence properties, WS_2 QDs can provide excellent sensitivity, specificity, and reliability across a broad range of applications, contributing to advancements in technology, health, safety, and environmental protection.[41–43] The WS_2 QD-based sensors can be used for environmental monitoring. Heavy metals like Pb, Hg, and Cd and other organic pollutants like dyes, present in water and soil, can be detected by using WS_2

Table 1 Comparative assessment of WS_2 QDs relative to other materials addressed in the literature for determination of OFL and CIP

Method		Materials	Range	LOD		LOQ		Ref.
				OFL	CIP	OFL	CIP	
Electrochemical		ZnO/GR/GCE	1–100 μM	0.33 μM	—	—	—	55
Electrochemical	LSV	MoS_2@MWCNT	0.24–0.82 μM	0.17 μM	—	0.56 μM	—	48
	DPNV		0.29–0.82 μM	0.12 μM	—	0.4 μM	—	
Electrochemical (SWAdASV)		$[FG_2/MW_2]$/CPE	6×10^{-4}–1.5×10^{-2} μM	0.18 nM	—	—	—	49
Electrochemical (amperometry)		Cu_2O/NG	0.5–27.5 μM	0.34 μM	—	—	—	47
Ratiometric fluorescence		Tb–Eu-MOG	0.3–24 μM	—	90 nM	—	—	51
Ratiometric fluorescence		CD/riboflavin	0.5–200 μM	—	0.13 μM	—	—	54
Fluorescence		Eu–Ga-MOF	30–600 μM	—	7250 μM	—	—	53
Fluorescence		CdSe QDs	0–120 μM	—	0.6 μM	—	—	52
Fluorescence		WS_2 QDs	0 μM to 3 μM	0.08 μM	0.06 μM	0.26 μM	0.21 μM	This work

SWAdASV – square-wave adsorptive anodic stripping voltammetry, DPNV – differential pulse normal voltammetry, LSV – linear sweep voltammetry.

QDs. They can detect harmful pesticide residues, pathogens, and viruses in food, preventing foodborne diseases.[44] They can detect plant stress markers and diseases, supporting the early intervention and management of crop health. Additionally, these sensors are employed in imaging techniques to observe cellular structures and functions and can measure pH levels in biological and chemical processes contributing to medical research and diagnostics.[33,45] Also, these sensors are utilized for gas sensing such as NH_3, NO_2, and CO detection for air quality monitoring and safety measures.[46]

Comparative study

The comparative analysis of the current research on WS_2 QDs with different previously reported[47–54] nanomaterials, utilized for analytical determination of ofloxacin and ciprofloxacin, is displayed in Table 1. The key factors included were the materials used, detection method, detection range, LOD, and LOQ. This demonstrated that our WS_2 QDs exhibit lower detection and quantification limits with a competitive linear range for the determination of FQns (OFL and CIP) compared with most of the reported methods. Also, our system detects both OFL and CIP giving great LOD and LOQ results, whereas all other reported systems are showing detection of either OFL or CIP and giving only LOD results without a quantification limit but MoS_2@MWCNT is an exception[48] which is an advantage. Some materials used for sensing OFL and CIP were expensive lanthanide-based composites. Our material is cost-effective with low toxicity and we are using a single-step process to prepare this material; also, the detection method is user-friendly which encourages its potential for commercialization in the future. Furthermore, the method achieved superior sensitivity to many persisting approaches and bridged the gap among various methods within this sensing range.

Disposal strategy for WS_2 QD-based sensors/WS_2 QDs

Developing and implementing effective disposal strategies for WS_2 QDs and other sensors/materials are essential for minimizing their environmental and health impacts. Some components of sensors, such as QDs, may contain heavy metals (Pb, Hg, Cd) or other toxic substances.[56] Improper disposal of these materials can lead to soil and water contamination, potentially causing long-term impacts on the environment and human health, as these kinds of materials are often chemically stable and can persist in the environment for long periods. So, effective disposal strategies for sensors and materials are crucial for responsible research and practical implementation. Focusing on recycling and reusing components of WS_2 QDs with diverse strategies and following regulatory guidelines assure that these advanced materials can contribute to technological progress without compromising environmental sustainability.

Although direct recycling of WS_2 QDs may be challenging due to their stability and tiny size, methods like solvent extraction can be applied for this purpose by using some specific polar aprotic solvents like DMF, DMSO, and NMP to dissolve WS_2 QDs from used products. This allows the recovery of WS_2 for reuse in the production of new quantum dots. Aqueous solutions with surfactants or mixed solvent systems can also be used to enhance dispersion and extraction efficiency. Controlled thermal processes can decompose WS_2 QDs, enabling the separation and recovery of tungsten and sulfur for reuse. Devices or materials containing WS_2 QDs can be mechanically disassembled, and the quantum dots can be separated using centrifugation or filtration techniques. Wherever recycling is not feasible, WS_2 QDs should be disposed of in designated facilities following local guidelines for hazardous materials. Additionally, developing WS_2 QD-based sensors by applying biocompatible and environmentally friendly coatings can enhance their recyclability and reduce their environmental impact during disposal.

Conclusion

We have developed a fluorescent turn-on sensor based on WS_2 QDs. It shows exceptional results in sensitivity, specificity, and feasibility toward FQns (OFL and CIP) in water. The FL emission intensity of WS_2QDs interacting with FQns (OFL and CIP) showed a systematic linear enhancement and peak shifting on varying FQn concentrations from 0 μM to 3 μM and thus can be potentially used for the quantification of OFL and CIP. The obtained WS_2 QDs are the first example of TMD QDs without further modification that can function as a super responsive and selective fluorescent sensor to determine FQns (OFL, and CIP) with minimum detectable amounts to the extent of 0.08 μM and 0.06 μM for OFL and CIP, respectively; also, their respective minimum quantification limits were found to be 0.26 μM and 0.21 μM. In comparison to the reported literature, our sensor for monitoring FQns (OFL, CIP) has a very systematic way along with a linear range, also exhibits an extremely low sensitivity threshold, and can function as an exceptionally efficient fluorescent sensor. Also, it can sensitively detect and quantify both OFL and CIP at very low concentrations. Therefore, this strategy has potential for advancing new approaches for practical identification and biochemical testing of FQns (OFL and CIP).

Notes

Abbreviations

QDs	Quantum dots
WS_2 QDs	Tungsten disulfide quantum dots
FQns	Fluoroquinolones
OFL	Ofloxacin
CIP	Ciprofloxacin
NFX	Norfloxacin
LOD	Limit of detection
LOQ	Limit of quantification
TMDs	Transition metal dichalcogenides
$MoSe_2$	Molybdenum diselenide

WSe_2	Tungsten diselenide
L-Cys	L-Cysteine
XRD	X-ray diffraction
TEM	Transmission electron microscopy
UV-vis	Ultraviolet and visible
FTIR	Fourier transform infrared
SAED	Selected area electron diffraction
FL	Fluorescence

Data availability

The data supporting the findings of this study are available within the article and its ESI.† Additional data that support the findings of this study are available from the corresponding author upon reasonable request.

Author contributions

C. U. and S. B. conceived the idea and designed the experiments. S. B. performed the experiments and also drafted and edited the manuscript. C. U. edited and finalized the manuscript.

Conflicts of interest

The authors declare no competing financial interest.

Acknowledgements

S. B. would like to thank the Department of Science and Technology (DST INSPIRE) for providing the DST-INSPIRE Fellowship. The authors also extend their thanks to the Central Instrument Facility IIT, (BHU) Varanasi for instrument facilities.

References

1 S. Wu, P. Hua, D. Gui, J. Zhang, G. Ying and P. Krebs, *Water Resour. Res.*, 2022, **225**, 119138.
2 E. Bora, C. R. Upadhyay and A. V. Koncagül, *Water for prosperity and peace The United Nations World Water Development Report 2024 Executive Summary*, 2024.
3 N. B. Jadeja, T. Banerji, A. Kapley and R. Kumar, *Water Security*, 2022, **16**, 100119.
4 B. Eryildiz, B. Y. Gul and I. Koyuncu, *J. Water Process Eng.*, 2022, **49**, 103036.
5 V. Bressi, C. Celesti, A. Ferlazzo, T. Len, K. Moulaee, G. Neri, R. Luque and C. Espro, *Environ. Sci.: Nano*, 2024, **11**, 1245–1258.
6 X. Tong, X. Lin, N. Duan, Z. Wang and S. Wu, *ACS Sens.*, 2022, **7**, 3947–3955.
7 V. Vinayagam, S. Murugan, R. Kumaresan, M. Narayanan, M. Sillanpää, N. V. Dai Viet, O. S. Kushwaha, P. Jenis, P. Potdar and S. Gadiya, *Chemosphere*, 2022, **300**, 134597.
8 M. M. Sabzehmeidani and M. Kazemzad, *Sci. Total Environ.*, 2022, **810**, 151997.
9 B. Tan, H. Zhao, L. Du, X. Gan and X. Quan, *Biosens. Bioelectron.*, 2016, **83**, 267–273.
10 J. Van der Geer, J. A. J. Hanraads and R. A. Lupton, *J. Sci. Commun.*, 2000, **163**, 51–59.
11 H. H. Cho, D. H. Jung, J. H. Heo, C. Y. Lee, S. Y. Jeong and J. H. Lee, *ACS Appl. Mater. Interfaces*, 2023, **15**, 19785–19806.
12 J. Liu, Y. Li, L. Liu, Y. Gao, Y. Zhang, Z. Yin, F. Pi and X. Sun, *Bull. Environ. Contam. Toxicol.*, 2021, **107**, 176–184.
13 Y. Ye, T. Wu, X. Jiang, J. Cao, X. Ling, Q. Mei, H. Chen, D. Han, J.-J. Xu and Y. Shen, *ACS Appl. Mater. Interfaces*, 2020, **12**, 14552–14562.
14 K. J. Aldred, R. J. Kerns and N. Osheroff, *Biochemistry*, 2014, **53**, 1565–1574.
15 L. Xu, H. Li, P. Yan, J. Xia, J. Qiu, Q. Xu, S. Zhang, H. Li and S. Yuan, *J. Colloid Interface Sci.*, 2016, **483**, 241–248.
16 T. Liu, Q. Xue, J. Jia, F. Liu, S. Zou, R. Tang, T. Chen, J. Li and Y. Qian, *Phys. Chem. Chem. Phys.*, 2019, **21**, 16282–16287.
17 R. Aggarwal, A. K. Garg, V. Kumar, H. Jonwal, S. Sethi, S. Gadiyaram, S. K. Sonkar, A. K. Sonker and G. Westman, *ACS Appl. Nano Mater.*, 2023, **6**, 6518–6527.
18 L. Xu, H. Li, P. Yan, J. Xia, J. Qiu, Q. Xu, S. Zhang, H. Li and S. Yuan, *J. Colloid Interface Sci.*, 2016, **483**, 241–248.
19 L. Shi, X. Zou, T. Wang, D. Wang, M. Fan and Z. Gong, *Chin. Chem. Lett.*, 2022, **33**, 442–446.
20 J. A. M. Pulgarín, A. A. Molina and N. Boras, *Anal. Methods*, 2012, **4**, 3413–3419.
21 X. Mu, S. Zhang, J. Lu, Y. Huang and J. Ji, *J. Hazard. Mater.*, 2024, **470**, 133740.
22 M. Wang, L. He, X. Zheng, Y. Lin, F. Xie, S. Xiao, Z. Chen and Q. Cai, *J. Food Compos. Anal.*, 2024, **127**, 105969.
23 W. Yu, S. Zhan, Z. Shen, Q. Zhou and D. Yang, *Chem. Eng. J.*, 2017, **313**, 836–846.
24 X. H. Zhang, Y. Deng, M. Z. Zhao, Y. L. Zhou and X. X. Zhang, *RSC Adv.*, 2018, **8**, 4063–4071.
25 V. D. Dang, A. B. Ganganboina and R. A. Doong, *ACS Appl. Mater. Interfaces*, 2020, **12**, 32247–32258.
26 C. Wang, F. Qin, S. Tang, X. Li, T. Li, G. Guo, C. Gu, X. Wang and D. Chen, *Food Chem.*, 2023, **411**, 135514.
27 A. Rateb, Z. Ghubish, A. F. Abdel Hakiem and M. El-Kemary, *J. Photochem. Photobiol., A*, 2023, **443**, 114867.
28 V. K. Singh, H. Mishra, R. Ali, S. Umrao, R. Srivastava, S. Abraham, A. Misra, V. N. Singh, H. Mishra and R. S. Tiwari, *ACS Appl. Nano Mater.*, 2018, **2**, 566–576.
29 L. Lin, Y. Xu, S. Zhang, I. M. Ross, A. C. M. Ong and D. A. Allwood, *ACS Nano*, 2013, **7**, 8214–8223.
30 N. P. Mani and J. Cyriac, *New J. Chem.*, 2020, **44**, 10840–10848.
31 F. Ghribi, A. Alyamani, Z. Ben Ayadi, K. Djessas and L. E. L. Mir, *Energy Procedia*, 2015, **84**, 197–203.
32 D. Günder, M. Axt and G. Witte, *ACS Appl. Mater. Interfaces*, 2024, **16**, 1911–1920.
33 T. Song, Q. Wang, H. Yu, W. Gao, Y. Xu, Y. Lv, Y. Xing, Y. Chen and M. Yang, *Anal. Bioanal. Chem.*, 2022, **414**, 1623–1630.
34 F. Yan, Z. Sun, J. Xu, H. Li and Y. Zhang, *Microchim. Acta*, 2020, **187**, 1–9.
35 K. Zhang, L. Fu, W. Zhang, H. Pan, Y. Sun, C. Ge, Y. Du and N. Tang, *ACS Omega*, 2018, **3**, 12188–12194.

36 V. Selamneni, P. Anand P, A. Singh and P. Sahatiya, *ACS Appl. Electron. Mater.*, 2021, **3**, 4105–4114.
37 A. Bora, L. P. L. Mawlong, R. Das and P. K. Giri, *J. Colloid Interface Sci.*, 2020, **561**, 519–532.
38 S. W. Zheng, L. Wang, H. Y. Wang, C. Y. Xu, Y. Luo and H. B. Sun, *Nanoscale*, 2021, **13**, 17093–17100.
39 L.-S. Feng, M.-L. Liu, S. Zhang, Y. Chai, B. Wang, Y.-B. Zhang, K. Lv, Y. Guan, H.-Y. Guo and C.-L. Xiao, *Eur. J. Med. Chem.*, 2011, **46**, 341–348.
40 A. M. Naglah, M. A. Al-Omar, A. A. Almehizia, H. M. AlKahtani, M. A. Bhat, N. S. Al-Shakliah, K. Belgacem, B. M. Majrashi, M. S. Refat and A. M. A. Adam, *J. Mol. Struct.*, 2021, **1225**, 129102.
41 W. Yin, X. Bai, P. Chen, X. Zhang, L. Su, C. Ji, H. Gao, H. Song and W. W. Yu, *ACS Appl. Mater. Interfaces*, 2018, **10**, 43824–43830.
42 F. Yan, Z. Sun, J. Xu, H. Li and Y. Zhang, *Microchim. Acta*, 2020, **187**, 344.
43 T. Song, Q. Wang, H. Yu, W. Gao, Y. Xu, Y. Lv, Y. Xing, Y. Chen and M. Yang, *Anal. Bioanal. Chem.*, 2022, **414**, 1623–1630.
44 Y. Sun, W. Liu, M. Chen, H. Ji, M. Jiang, Z. Hao, X. Li, S. He, L. Zhang and R. Zhang, *Green Chem.*, 2024, **26**, 7123–7131.
45 D. R. Hang, D. Y. Sun, C. H. Chen, H. F. Wu, M. M. C. Chou, S. E. Islam and K. H. Sharma, *Nanoscale Res. Lett.*, 2019, **14**, 271.
46 C. Ouyang, Y. Chen, Z. Qin, D. Zeng, J. Zhang, H. Wang and C. Xie, *Appl. Surf. Sci.*, 2018, **455**, 45–52.
47 F. Wu, F. Xu, L. Chen, B. Jiang, W. Sun and X. Wei, *Chem. Res. Chin. Univ.*, 2016, **32**, 468–473.
48 R. Sharma, S. Kumar, D. S. Rana, S. Thakur, N. Gupta and D. Singh, *J. Environ. Chem. Eng.*, 2024, **12**, 112413.
49 M. Elfiky, N. Salahuddin, A. Hassanein, A. Matsuda and T. Hattori, *Microchem. J.*, 2019, **146**, 170–177.
50 J. Hua, Y. Jiao, M. Wang and Y. Yang, *Microchim. Acta*, 2018, **185**, 137.
51 Y. Sun, P. Dramou, Z. Song, L. Zheng, X. Zhang, X. Ni and H. He, *Microchem. J.*, 2024, **26**, 7123–7131.
52 H. Xia, M. Peng, N. Li and L. Liu, *Chem. Phys. Lett.*, 2020, **740**, 137085.
53 B. Wang and B. Yan, *Talanta*, 2020, **208**, 120438.
54 C. Lu, G. Liu, Z. Yang, Y. Wang, H. Rao, W. Zhang, B. Jing and X. Wang, *Microchim. Acta*, 2020, **187**, 1–9.
55 X. Si, Y. Wei, C. Wang, L. Li and Y. Ding, *Anal. Methods*, 2018, **10**, 1961–1967.
56 F. Mashkoor, R. Mashkoor, M. Shoeb, A. H. Anwer, M. Z. Ansari and C. Jeong, *Appl. Clay Sci.*, 2023, **245**, 107149.